Supplementary Material for:
Effective sorting of fractional optical vortex modes

Zhengyang Mao, [a,†] Haigang Liu, [a,†,*] and Xianfeng Chen [a,b,*]

[a]State Key Laboratory of Advanced Optical Communication Systems and Networks, School of Physics and Astronomy, Shanghai Jiao Tong University, Shanghai 200240, China
[b]Shanghai Research Center for Quantum Sciences, Shanghai 201315, China

Abstract. Mode sorter is the crucial component of the communication systems based on orbital angular momentum (OAM). However, schemes proposed so far can only effectively sort integer OAM (IOAM) modes. Here, we demonstrate the effective sorting of fractional OAM (FOAM) modes by utilizing the coordinate transformation method, which can convert FOAM modes to IOAM modes. The transformed IOAM modes are subsequently sorted by using a mode conversion method called topological charge matching. The validation of our scheme is verified by implementing two FOAM sorting processes and corresponding mode purity analyses, both theoretically and experimentally. This new sorting method exhibits a huge potential of implementing a highly confidential and high-capacity FOAM-based communication and data-storage system, which may inspire further applications in both classical and quantum regimes.

Keywords: vortex mode sorter, fractional vortex beam, angular momentum, coordinate transformation.

*Haigang Liu, Email: liuhaigang@sjtu.edu.cn; Xianfeng Chen, Email: xfchen@sjtu.edu.cn
†These authors contributed equally to this work

1 Details about the coordinate transformation and the transformation phase Q_1

To begin with, the optical coordinate transformation method is based on the General Snell's Law (GSL) in ray optics. The GSL points out that, when a light beam passes through an interface, the refractive angle of the output beam is determined by the refractive index and the phase gradient of the interface, which is given by

$$n_t sin\theta_t - n_i sin\theta_i = \frac{1}{k}\frac{\partial Q}{\partial x}, \tag{S1}$$

where n and θ is the refractive index and the angle, k is the wave vector in free space and Q is the phase distribution on the interface. t and i means the refracted beam and the input beam respectively, as shown in Fig. S1(a). Next, we consider the propagation of a parallel light between two planes in free space showed in Fig. S1(b), where there is a distance d between the input plane (x, y) and the output plane (u, v). The input light on (x, y) on the input plane will be refracted and locate on (u, v) on the output plane. The relationship between the two points is determined by Eq.

(S1). If the incident beam is perpendicular to the input plane ($\theta_i = 0$) and the propagation is paraxial ($sin\theta_t \approx \theta_t = \frac{u-x}{d}$), the GSL can be simplified as the formulas

$$\mathcal{Q}_x = k(n_t sin\theta_t - n_i sin\theta_i) \approx k\theta_t = k\frac{u-x}{d}, \mathcal{Q}_y = k\frac{v-y}{d}, \quad \text{(S2)}$$

where $\mathcal{Q}(x, y)$ is the transformation phase loaded on the input plane and $\mathcal{Q}_x$ and $\mathcal{Q}_y$ are the partial derivatives with respect to (x, y). Therefore, the mapping rule between (x, y) and (u, v) is totally determined by $\mathcal{Q}$. And the phase $\mathcal{Q}$ can be easily obtained by substituting the mapping rule into Eq. (S2) and calculating the integral. In our method, the mapping rule is a spiral-to-spiral rule. The input field is separated by several spirals and mapped onto another group of spirals on the output plane. Figure S1(c) is the schematic of our coordinate transformation and clearly illustrates the mapping from spirals to spirals. The input vortex field is divided by two groups of curves. Group 1 (blue) consists of a small circle and a spiral, and group 2 (red) consists of a large circle and the same spiral. The region between the two sets of curves completely covers the entire vortex field. After the transformation, each group of curves is located on a new spiral. These two new spirals meet head to tail and form a closed area.

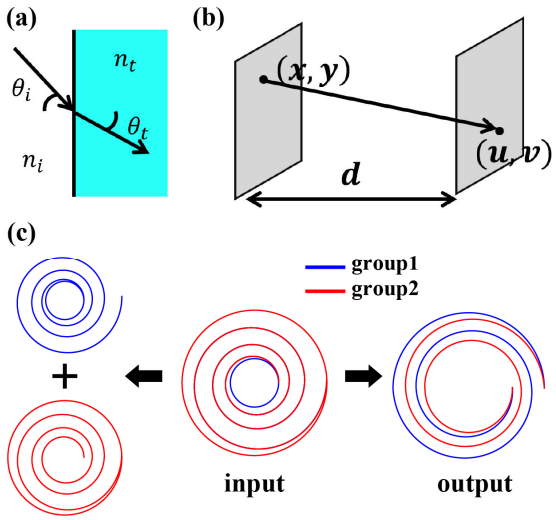

Fig. S1 (a) The General Snell's Law. (b) Coordinate mapping between two planes. (c) Schematic of the spiral-to-spiral transformation.

In order to better describe the mapping rule and calculate the corresponding phase, the input plane is redefined in terms of spiral-polar coordinate described by the radial coordinate r and the spiral azimuthal coordinate θ varies in $[0, +\infty)$. Similarly, the output plane is redefined by ρ and φ. Then the mapping rule in our method is described by (Eq. (2) of the main text):

$$\rho = cr^{-1/n}, \varphi = \theta/n, \tag{S3}$$

where c is an arbitrary constant and n is the transformation factor. The simplified GSL formulas Eq. (S2) written in the Cartesian coordinate should be rewritten in the spiral-polar coordinate, which is

$$\frac{\partial Q}{\partial r} = \frac{k}{d}(\rho\cos(\varphi-\theta) - r), \frac{\partial Q}{\partial \theta} = \frac{k}{d} r\rho\sin(\varphi-\theta), \tag{S4}$$

Then by substituting Eq. (S3) and calculating the integral of Eq. (S4), the transformation phase Q_1 can be easily obtained (Eq. (3) of the main text). The calculation of the correction phase Q_2 is detailed in the main text.

The additional correction phase $\mathcal{P}$ is introduced to compensate for the discontinuous points in the azimuthal phase of the output mode. As the middle column of Fig. 1 shows, the position of the mth discontinuous point is $\varphi_m = m\frac{2\pi}{n}$ $(m = 0,1,2\ldots)$. The output plane is divided into several regions by these points and the mth region is between two neighboring discontinuous points φ_m and φ_{m+1}. Therefore, the point (ρ, φ) is on the region labeled by $\left[\frac{n\varphi}{2\pi}\right]$. The phase difference on the discontinuous point is determined by the input mode, which is $\mathcal{P}_0 = 2\pi mod(\ell_{in}, 1)$. The compensation is to make up the region after the point. However, different regions require different phase compensation, because if we add $\mathcal{P}_0$ to the first region, the second region needs $2\mathcal{P}_0$ to compensate. Finally, the additional correction phase $\mathcal{P}$ is

$$\mathcal{P}(\rho, \varphi) = \mathcal{P}_0 \times \left[\frac{n\varphi}{2\pi}\right] = 2\pi t \left[\frac{n\varphi}{2\pi}\right], \tag{S5}$$

where $t = mod(\ell_{in}, 1)$.

2 Details about the correction phase $\mathcal{P}$

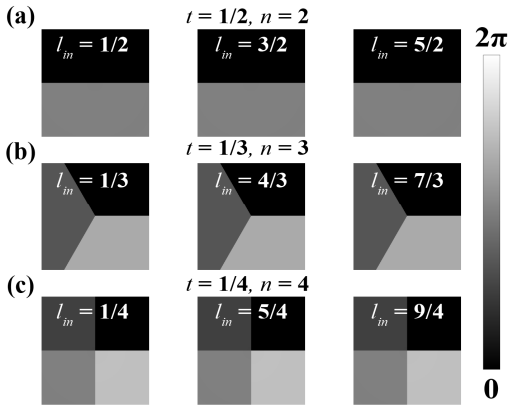

Fig. S2 The additional correction phase $\mathcal{P}$ for different parameters (a) $t = 1/2,\ n = 2$. (b) $t = 1/3,\ n = 3$. (c) $t = 1/4,\ n = 4$.

The additional correction phase $\mathcal{P}$ is expressed as

$$\mathcal{P}(\rho, \varphi) = 2\pi t \left[\frac{n\varphi}{2\pi}\right], \tag{S6}$$

where $t = mod(\ell_{in}, 1)$. $\mathcal{P}$ remains identical for the same t, indicating one correction phase $\mathcal{P}$ can be applied to a set of FOAM modes with the same t instead of with the same ℓ_{in}, such as all half-integer FOAM modes ($\ell_{in} = 1.5, 2.5, 3.5$ ...) with $t = 0.5$. Consequently, the same corrected phase distribution does not work only for a particular incident light beam. In the practical applications, we can use such a group of FOAM modes to realize FOAM communication system. Simultaneously, this feature also inherently provides encryption to the communication system, where the efficient sorting relies on the t-dependent coordinate transformation which acts as the encryption key. Figure S2 shows some different corrected phase distributions superimposed on the spiral transformation. It is clearly that the phase distribution is the same for FOAM modes with the same t.

3 The effect of the spiral's parameters on spiral transformation

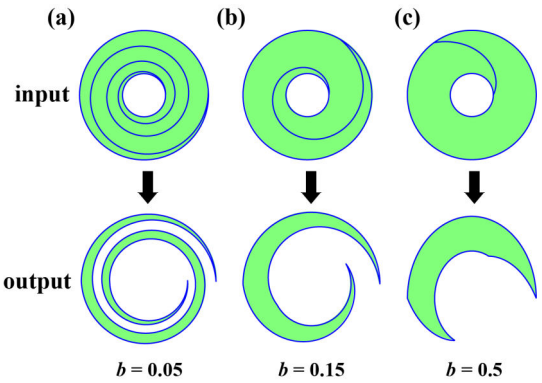

Fig. S3 The transformation results with (a) $t = 1/2,\ n = 2$. (b) $t = 1/3,\ n = 3$. (c) $t = 1/4,\ n = 4$.

The spiral used in our method is the logarithmic spiral defined by

$$r = ae^{b\theta}, \theta \in [0, \infty) \tag{S7}$$

where a is the initial radial position and b is the exponential growth rate. In our coordinate transformation method, the input field is separated by this spiral and mapped onto another spiral on the output plane which is defined by

$$\rho = ca^{-1/n}e^{-b\varphi}, \tag{S8}$$

The parameters a determines the position of the spiral while b determine the shape of the spiral. Figure S3 illustrates the transformation results with different parameters, in which the green region represents the vortex field. Figure S3(a) shows one successful mode conversion with appropriate parameters. The successful mode conversion requires that the input vortex field can be completely split by the spiral and that the output field can form a complete vortex shape. Specifically speaking, the classical vortex field is a halo pattern surrounded by two circles with two different radii. In order to meet the first requirement, the parameter a should be close to the inner radius. If a is close to or even larger than the outer radius, the segmentation of the incident vortex light field is invalid. For the second requirement, the parameter b needs to be in a suitable range. b determines the growth rate of the spiral's radius. A large b will result in a small number of turns of the spiral within the vortex field, leading to an incomplete output vortex pattern as shown in Figs. S3(b)-S3(c). It is worth mentioning that, the segmentation becomes finer with a smaller b, but this will be limited by the resolution of the phase modulation element. Therefore, b needs to be in a suitable range in experiment.

4 The calculation of the crosstalk between different OAM modes

The overlap integral between the optical fields is calculated by the formula[50]

$$c_{21} = \iint E_2^*(x,y)E_1(x,y)dxdy\,, \tag{S9}$$

which expresses the crosstalk amplitude between OAM mode 1 and OAM mode 2. Thus, the relative crosstalk power can be expressed as

$$C_{21} = \left|\frac{c_{21}}{c_{11}}\right|^2, \tag{S10}$$

Considering that in the real experiments we will separate different modes by spatial filtering, the integration region is the central region of the whole optical field with a radius of 100 μm, which is consistent with the radius of spatial filter. The obtained crosstalk matrix[51] is shown in Fig. S4, which proves that the crosstalk between different FOAM modes is very low when using a spatial filter for sorting.

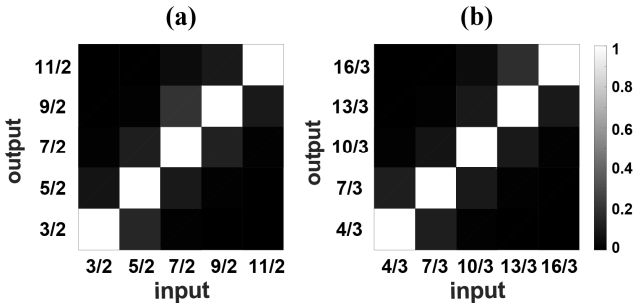

Fig. S4 The crosstalk matrix C_{out-in} for (a) $t = 1/2,\ n = 2$. (b) $t = 1/3,\ n = 3$.

5 Principle of the OAM mode purity analysis

The beams extracted by our method are further analyzed by purity analysis. Basically, the output field can be expanded and represented by a linear combination of basis IOAM modes following the equation

$$E(\rho, \varphi) = \sum_{\ell=-\infty}^{+\infty} a_\ell(\rho)\exp(i\ell\varphi). \tag{S11}$$

Therefore, the complex coefficient for topological charge ℓ can be calculated as

$$a_\ell(\rho) = \int_0^{2\pi} E(\rho, \varphi)\exp(-i\ell\varphi)\,\mathrm{d}\varphi. \tag{S12}$$

And the intensity and the corresponding mode purity of the OAM mode with topological charge ℓ is

$$I_\ell = \int_0^{+\infty} |a_\ell(\rho)|^2 \rho \mathrm{d}\rho,\ \ P_\ell = I_\ell / \sum_{q=-\infty}^{+\infty} I_q \tag{S13}$$

In our experiment, this process is performed by using an OAM detection system consists of SPP, L7, and CCD. SPP with topological charge ℓ is used to superimpose the basis IOAM mode on the output field. The Fourier transformation on the resultant field is performed using L7 which is positioned away from the SPP with a distance of f. The intensity distribution at the Fourier plane is recorded using CCD. The on-axis intensity shows the intensity of $-\ell$th-order OAM mode. In practical experiment, the on-axis intensity is the average intensity in the central region, which is determined by the central Gaussian-like spot obtained under the condition of matching. By replacing different SPPs, we can obtain the intensities of different OAM modes and calculate the corresponding purities.